Determination of the Van Hove Spectrum of Liquid He(4): An Application of the Feynman−Kleinert Linearized Path Integral Methodology†

Jens Aage Poulsen* and Gunnar Nyman

Physical Chemistry, Göteborg University, S-412-96, Göteborg, Sweden

Peter J. Rossky

Institute for Theoretical Chemistry, Department of Chemistry and Biochemistry, University of Texas at Austin, Austin, Texas 78712

Received: February 17, 2004

The spectrum of the Van Hove correlation function (CF) is calculated for liquid He(4) at 27 K and a density of 0.25 g/cm^3 by utilizing a recently proposed approximation to quantum CFs derived by combining an effective-frequency Boltzmann−Wigner transform with a linearized path integral expression for CFs. For this anharmonic system and highly nonlinear CF, we obtain excellent agreement with available accurate results. In particular, the first, second, and third moments of the spectrum are in very good agreement with both experiment and earlier theoretical results. Also, the calculated kinetic energy is in excellent agreement with accurate path integral Monte Carlo results.

1. Introduction

During the past decade, significant progress has been made in developing practical methods for calculating the dynamics of many-body quantum systems. These methods can roughly be divided into pure quantum methods and semi/quasiclassical methods, the last group representing methods which utilize some form of classical mechanics. In the first family we find, e.g., path integral Monte Carlo (PIMC) analytical continuation approaches based on maximum entropy schemes[4,28] and a PIMC quantum mechanical mode-coupling theory for liquids.[29] The last family includes a diverse set of simulation algorithms, such as centroid molecular dynamics (CMD),[17] the semiclassical initial value representation (SC-IVR) of correlation functions (CFs),[23] forward−backward semiclassical dynamics,[25,36] and the classical Wigner (CW) or, equivalently, the linearized semiclassical initial value representation (LSC-IVR) of CFs.[23,26]

The accuracy, computational cost, and range of validity of these methods differ substantially as one goes from one algorithm to another. For example, the two PIMC schemes of family one have been shown to accurately describe quantum diffusion of liquid *p*-hydrogen at low temperatures.[28,29] The computational workload of these methods is, however, large: The total number of PIMC beads is on the order of 10 000, and the number of MC steps is one to several millions.[28,29] Also, these two methods have different ranges of validity: Maximum entropy methods cannot resolve sharp peaks in quantum spectra,[4] while the mode-coupling theory is a high-density theory. The more economical but more approximate methods are found in the second family. Here, the undoubtedly most accurate theory is the SC-IVR method of Miller.[23] SC-IVR and its forward−backward analogue have been shown to nearly quantitatively account for quantum interference effects in many contexts such as diffraction and in the calculation of flux-side CFs, see ref 23, but the implementation is challenging due to the required propagation of monodromy matrix elements and the existence of rapidly oscillatory phases in the semiclassical propagator. It appears that SC-IVR is still not practical for large systems such as liquids.

Until recently, only CMD has been applied to realistic condensed-phase systems, for instance, in the context of vibrational energy relaxation (VER)[16] and in the study of the structure of water.[21] CMD has been found to accurately describe transport,[6,18,37] but it is a specialized theory, being rigorously formulated only for linear CFs.[17] Very recently, Makri and coworkers have reported forward−backward semiclassical calculations on argon[36] and *p*-hydrogen[25] liquids. Their forward−backward approach was found to suffer slightly from a weakly oscillatory integrand, thereby making the scheme practical for either low-dimensional systems or moderate temperature, unless additional approximations are adopted.[25] The forward−backward scheme was shown to accurately describe the quantum diffusion of liquid *p*-hydrogen at temperatures over 20 K.[25] Shi and Geva also very recently reported on an implementation of the CW method in a realistic condensed-phase context and successfully applied it to the challenging problem of the VER of oxygen in liquid oxygen.[30,31] These most recent developments are indeed exciting since the underlying methods are computationally quite practical and, perhaps most importantly, general. Their main disadvantage is that they capture only short time-interference effects. One may however argue that, for the determination of CFs in liquids, this is not a serious problem due to decoherence.[11,14,26] In this paper, we will explore further the ability of one of these "low cost" methods, the CW method, to predict the quantum dynamics of a real liquid.

The CW approach, the subject of this paper, requires the Wigner transform of the Boltzmann operator when calculating CFs in the canonical ensemble. The implementation of this Wigner transform is a nontrivial problem for large systems where basis-set methods cannot be applied. This is the main reason the approach has not been explored in realistic condensed-phase applications, except for the pioneering study of Shi and Geva who used a novel harmonic approximation to the Boltzmann operator.[30] Quite recently, we suggested a different

† Part of the "Gert D. Billing Memorial Issue".

10.1021/jp049281d CCC: $27.50
Published on Web 06/02/2004

route to the required Wigner transform of the $\exp(-\beta\hat{H})\hat{A}$ operator.[26] This approach combines the novel effective-frequency variational theory, developed independently by Giachetti and Tognetti[12,13] and by Feynman and Kleinert,[10] with the quasidensity operator formalism of Jang and Voth.[17] This implementation of the Boltzmann−Wigner transform[26] is practical for systems with up to hundreds of interacting atoms and could therefore enable the simulation of many nontrivial systems if the CW method is reliable. Comparisons between CW and experiment are thus highly desirable to gain insight into its value as a computational tool for quantum liquids.

This paper reports the results of our CW implementation when applied to the determination of the Van Hove spectrum, $S(\vec{Q},\omega)$, of He(4) at 27 K and a density of 0.25 g/cm^3. The experimental inelastic X-ray spectrum (IXS) of the He(4) scattering function at this thermodynamic point has been reported by Verbeni and co-workers.[34] There has been other related theoretical work. CMD has previously been used by Kinugawa and co-workers for the purpose of obtaining the Van Hove spectrum of nonsuperfluid He(4)[24] at 4 K and liquid *p*-hydrogen at 14.7 K.[18] For small wave vectors, $\vec{Q}$, the agreement was found to be good, but as the magnitude increased, CMD performed increasingly worse.[24] This can be understood by observing that the nonlinearity of the Van Hove CF grows with increasing magnitude of $\vec{Q}$ and that CMD only provides a meaningful approximation to the Kubo transform of *linear* CFs.[17] The CW method, on the other hand, is completely free of this limitation. Ciccotti and co-workers[9] have previously applied a version of the CW method for obtaining the He(4) Van Hove spectrum at nearly the same thermodynamic point as considered in this paper. Very good agreement was observed between their calculated spectrum and the measurements of Verbeni et al. Their approach involved neglect of various oscillatory phase factors based on statistical arguments.

This paper is structured as follows: In section 2, the basic theory behind the CW method and our specific implementation of it is described. Also, the Van Hove correlation function is introduced as well as its spectral moments. In section 3, we mention the details behind the molecular dynamics simulation, and its predictions are presented in section 4. Finally, a short discussion of the results is found in section 5.

2. Theory

In this section, we discuss each of the theoretical components required for the present application.

2.1. The CW Method. The subject of this paper concerns the application and implementation of probably the simplest approach to the dynamics of large quantum systems, namely, the so-called CW or, equivalently, the LSC-IVR approach.[26,35] It can be summarized as follows. To obtain the CF $\langle\hat{A}(0)\hat{B}(t)\rangle$, one makes use of the approximate CW expression

$$\langle\hat{A}(0)\hat{B}(t)\rangle \approx \frac{1}{(2\pi\hbar)^{3N}}\frac{1}{Z}\int\int \mathrm{d}q\,\mathrm{d}p\,(\exp(-\beta\hat{H})\hat{A})_W[q,p](\hat{B})_W[q_t,p_t] \quad (1)$$

The interpretation/implementation of eq 1 goes as follows: Phase-space points (q,p) are sampled from the Wigner transform of $\exp(-\beta\hat{H})\hat{A}$, the transform being defined for an arbitrary operator $\hat{C}$ by

$$(\hat{C})_W[x,p] \equiv \int_{-\infty}^{+\infty}\mathrm{d}\eta\,\exp(-ip\eta/\hbar)\left\langle x+\frac{1}{2}\eta\left|\hat{C}\right|x-\frac{1}{2}\eta\right\rangle \quad (2)$$

(q,p) are evolved classically to (q_t,p_t), which serves as the phase-space arguments of $(\hat{B})_W[q_t,p_t]$. $3N$ is the dimensionality of the problem. As opposed to forward−backward schemes,[25] no Herman−Kluk coherent state parameters need be determined/optimized meaning that the CW method is parameter free. Recently, it was pointed out[26,32] that eq 1 could also be obtained by linearizing the exact path integral representation of the above CF without intermediate passage to an IVR CF. Hence it was suggested to term eq 1 a "linearized path integral (LPI) representation of CFs"[26] and not LSC-IVR. In the following, the three names CW, LSC-IVR and the LPI representation of CFs all refer to the identical approximation embodied in eq 1.

2.2. The Feynman−Kleinert Linearized Path Integral Implementation. Recently, we suggested a route to the Wigner transform of the $\exp(-\beta\hat{H})\hat{A}$ operator, as required by LPI.[26] This approach was based on combining the novel effective-frequency variational theory of Feynman and Kleinert (FK)[10] with the quasidensity operator formalism of Jang and Voth.[17] The resulting CF approach, called FK-LPI, can be summarized as follows.

In one dimension, one may approximate the Boltzmann operator by

$$\exp(-\beta\hat{H}) \simeq \int\int \mathrm{d}x_c\,\mathrm{d}p_c\,\rho_{FK}(x_c,p_c)\hat{\delta}_{FK}(x_c,p_c) \quad (3)$$

where $\rho_{FK}(x_c,p_c)$ is the FK approximation to the centroid density

$$\rho_{FK}(x_c,p_c) = \frac{1}{2\pi\hbar}\exp\left(-\beta\frac{p_c^2}{M}\right)\exp(-\beta W_1(x_c)) \quad (4)$$

and $W_1(x_c)$ is the corresponding FK approximation to the centroid potential. The operator $\hat{\delta}_{FK}(x_c,p_c)$ is the effective-frequency quasidensity operator

$$\hat{\delta}_{FK}(x_c,p_c) = \int\int \mathrm{d}x\,\mathrm{d}x'\left(\frac{M\Omega(x_c)}{\pi\hbar\alpha}\right)^{1/2}|x'\rangle\langle x|\times \exp\left\{\frac{p_c}{i\hbar}(x'-x) - \frac{M\Omega(x_c)}{\hbar\alpha}\left(\frac{x+x'}{2}-x_c\right)^2 - \frac{M\Omega(x_c)\alpha}{4\hbar}(x'-x)^2\right\} \quad (5)$$

where α is a function of the effective frequency, $\Omega(x_c)$, through

$$\alpha = \coth\left(\frac{\Omega(x_c)\hbar\beta}{2}\right) - \frac{2}{\Omega(x_c)\hbar\beta} \quad (6)$$

Wigner transforming eq 3 amounts to transforming $\hat{\delta}_{FK}$, eq 5, which can be done analytically

$$(\hat{\delta}_{FK}(x_c,p_c))_W[q,p] = \frac{2}{\alpha}\exp\left(-\frac{M\Omega(x_c)}{\hbar\alpha}(q-x_c)^2 - \frac{1}{M\Omega(x_c)\alpha\hbar}(p-p_c)^2\right) \quad (7)$$

If $\hat{A}$ is a simple operator, also the transform of $\exp(-\beta\hat{H})\hat{A}$ can be obtained. For details, we refer to ref 26. Before proceeding, we note that eqs 3−5 not only facilitate the analytical evaluation of the Boltzmann Wigner transform but equally well can be used for obtaining algebraic expressions for other quantum distribution functions such as, e.g., the Husimi distribution.[15] Insertion of eq 7 into the Wigner transform of eq 3, followed by an integration over p_c, yields the alternative formula (cf. eq 48 in ref 26)

$$(\exp(-\beta\hat{H}))_{\mathrm{W}}[q,p] = \int \frac{dx_{\mathrm{c}}}{2\pi\hbar}\,\rho_{\mathrm{FK}}(x_{\mathrm{c}})\,\frac{2}{\alpha}\left(\frac{M\alpha\pi}{\frac{\beta}{2}\coth(\hbar\Omega(x_{\mathrm{c}})\beta/2)}\right)^{1/2} \times \exp\left(-\frac{M\Omega(x_{\mathrm{c}})}{\hbar\alpha}(q-x_{\mathrm{c}})^2 - \frac{\tanh(\hbar\Omega(x_{\mathrm{c}})\beta/2)}{M\Omega(x_{\mathrm{c}})\hbar}p^2\right) \quad (8)$$

where $\rho_{\mathrm{FK}}(x_{\mathrm{c}}) = \exp(-\beta W_1(x_{\mathrm{c}}))$. The latter quantity allows for a classical-like calculation of the quantum partition function[20]

$$Z_{\mathrm{FK}} = \int \mathrm{d}x_{\mathrm{c}}\left(\frac{M}{2\beta\hbar^2\pi}\right)^{1/2}\rho_{\mathrm{FK}}(x_{\mathrm{c}}) \quad (9)$$

The performance of the LPI approach to CFs has been examined by Wang, Sun, and Miller in the context of obtaining reaction rate constants for a double-well particle coupled to a dissipative phonon bath.[33,35] They found that the LPI performed well with a bath coupling[35] but poorly without,[33] i.e., when long-time coherence effects become important. Essentially the same conclusions were drawn by Poulsen and co-workers[26] in their study of various CFs derived from LPIs in an anharmonic helium string study. The latter work further demonstrated the ability of FK-LPI to include quantum mechanical effects such as zero-point motion into a realistic simulation of liquid oxygen.

2.3. The Van Hove Correlation Function. For a simple liquid composed of N He(4) atoms, the Van Hove CF is given by[22]

$$S(\vec{Q},t) = \frac{1}{N}\sum_{j,k=1}^{N}\langle \exp(-i\vec{Q}\vec{r}_j(0))\exp(i\vec{Q}\vec{r}_{\mathrm{k}}(t))\rangle \quad (10)$$

where $\langle ...\rangle$ denotes a canonical ensemble average. We note the nonlinearity in $\vec{Q}$ that was pointed out earlier. For an isotropic liquid, the CF depends only on $||\vec{Q}||$. Its Fourier transform defines the Van Hove spectrum, $S(Q,\omega)$, through[22]

$$S(\vec{Q},\omega) = \frac{1}{2\pi}\int_{-\infty}^{+\infty}\mathrm{d}t\,\exp(-i\omega t)S(\vec{Q},t) \quad (11)$$

Moments of $S(\vec{Q},\omega)$ are defined by

$$\langle\omega^n\rangle = \int_{-\infty}^{+\infty}\mathrm{d}\omega\;\omega^n S(\vec{Q},\omega) \quad (12)$$

the first of which has the well-known exact value

$$\langle\omega\rangle = \hbar||\vec{Q}||^2/2M_{\mathrm{He(4)}} \quad (13)$$

To compare with experiment, we furthermore define "normalized" moments by

$$R^n = \frac{\hbar^n\langle\omega^n\rangle}{\hbar\langle\omega\rangle} = \hbar^{n-2}\frac{2M_{\mathrm{He(4)}}\langle\omega^n\rangle}{||\vec{Q}||^2} \quad (14)$$

and the *reduced* second moment by

$$\tilde{R}^2 = \left\{R^2 - \frac{\hbar^2||\vec{Q}||^2}{2M_{\mathrm{He(4)}}}\right\}\Big/2k_{\mathrm{B}}T \quad (15)$$

From eqs 14 and 15, it follows that the classical limit of $\tilde{R}^2$ is unity.

2.4. FK-LPI Equations. Here we utilize the FK-LPI theory developed in ref 26. In the following, we consider N He(4) atoms whose collective position vector is denoted by r. Similarly, for simplicity of notation, η, η_{c}, ν, ν_{c}, q, p, r_{c}, and p_{c} are all $3N$ dimensional vectors. To evaluate the FK-LPI approximation to the Van Hove CF, two Wigner transforms need to be evaluated, cf. eq 1

$$(\exp(-\beta\hat{H})\sum_{j=1}^{N}\exp(-i\vec{Q}r_j))_{\mathrm{W}}[q,p] \simeq \int\int \mathrm{d}r_c\,\mathrm{d}p_c\,\rho_{\mathrm{FK}}(r_{\mathrm{c}},p_{\mathrm{c}})(\hat{\delta}_{\mathrm{FK}}(r_{\mathrm{c}},p_{\mathrm{c}})\sum_{j=1}^{N}\exp(-i\vec{Q}r_j))_{\mathrm{W}}[q,p] \quad (16)$$

and

$$(\sum_{j=1}^{N}\exp(i\vec{Q}r_j))_{\mathrm{W}}[q_{\mathrm{t}},p_{\mathrm{t}}] = \sum_{j=1}^{N}\exp(i\vec{Q}q_{t,j}) \quad (17)$$

In the following, since He(4) is isotropic, we have the liberty of choosing the direction of $\vec{Q}$ to be along the x axis. Hence, we make the simplifications: $Q \equiv ||\vec{Q}||$ and the r_j vector is replaced by its x-axis component, $r_{x,j} \equiv r_j$ for particle j. Although the evaluation of eq 16 is in principle straightforward, it is rather lengthy, and an outline of its derivation is given in the Appendix. Here we just report the result where

$$\int\int \mathrm{d}r_c\,\mathrm{d}p_c\,\rho_{\mathrm{FK}}(r_{\mathrm{c}},p_{\mathrm{c}})(\hat{\delta}_{\mathrm{FK}}(r_{\mathrm{c}},p_{\mathrm{c}})\sum_{j=1}^{N}\exp(-iQr_j))_{\mathrm{W}}[q,p] = \int \mathrm{d}r_c\,\frac{\rho_{\mathrm{FK}}(r_{\mathrm{c}})}{(2\pi\hbar)^{3N}}\sum_{j=1}^{N}\exp(-iQq_j)\det(\mathbf{M}^{1/2})\prod_{n=1}^{3N}\frac{2}{\alpha_n}\left(\frac{\alpha_n\pi}{\frac{\beta}{2}\coth\left(\frac{\hbar\Omega_n(r_{\mathrm{c}})\beta}{2}\right)}\right)^{1/2}\exp\left(-\frac{1}{2}\lambda_n^{-1}(\eta_n-\eta_{n,\mathrm{c}})^2\right)\times \exp(-\mu_n\nu_n^2)\exp\left(\hbar\nu_n Q m_j^{-1/2}\mathbf{U}(r_{\mathrm{c}})_{3(j-1)+1,n}\mu_n - \frac{\hbar^2}{4}\mu_n Q^2 m_j^{-1}\mathbf{U}^2(r_{\mathrm{c}})_{3(j-1)+1,n}\right) \quad (18)$$

$$\lambda_n = \frac{k_{\mathrm{B}}T}{\Omega_n^2(r_{\mathrm{c}})}\left\{\frac{\hbar\Omega_n(r_{\mathrm{c}})}{2k_{\mathrm{B}}T}\coth\left(\frac{\hbar\Omega_n(r_{\mathrm{c}})}{2k_{\mathrm{B}}T}\right) - 1\right\} \quad (19)$$

and

$$\mu_n = \frac{\tanh(\hbar\beta\Omega_n(r_{\mathrm{c}})/2)}{\hbar\Omega_n(r_{\mathrm{c}})} \qquad \alpha_n = 2\lambda_n\Omega_n(r_{\mathrm{c}})/\hbar \quad (20)$$

In eq 18, we have utilized the centroid-dependent normal modes defined by

$$\eta = (\eta_1, ..., \eta_{3N})^T = \mathbf{U}^{\dagger}(r_{\mathrm{c}})\mathbf{M}^{1/2}q \quad (21)$$

$$\eta_{\mathrm{c}} = (\eta_{1,\mathrm{c}}, ..., \eta_{3N,\mathrm{c}})^T = \mathbf{U}^{\dagger}(r_{\mathrm{c}})\mathbf{M}^{1/2}r_{\mathrm{c}} \quad (22)$$

$$\nu = (\nu_1, ..., \nu_{3N})^T = \mathbf{U}^{\dagger}(r_{\mathrm{c}})\mathbf{M}^{-1/2}p \quad (23)$$

and

$$\nu_{\mathrm{c}} = (\nu_{1,\mathrm{c}}, ..., \nu_{3N,\mathrm{c}})^T = \mathbf{U}^{\dagger}(r_{\mathrm{c}})\mathbf{M}^{-1/2}p_{\mathrm{c}} \quad (24)$$

$\mathbf{M}$ is the $3N \times 3N$ matrix containing atomic masses m_i on the diagonal. For the definition of the centroid-dependent effective-frequency eigenvalues, $\Omega_n(r_{\mathrm{c}})$, and the real orthonormal matrix

$\mathbf{U}(r_c)$, see ref 26 and references therein. The practical scheme for sampling phase-space points from the above Wigner distribution then is: (i) Perform a Monte Carlo walk using the centroid density, $\rho_{FK}(r_c)$, thereby sampling positions r_c. (ii) Given a sampled position, a sampling of (q,p) is done by evaluating its corresponding weight factor defined by

$$W(q,p) = \sum_{n=1}^{3N} \frac{2}{\alpha_n} \left(\frac{\alpha_n}{\coth\left(\frac{\hbar\Omega_n(r_c)\beta}{2}\right)} \right)^{1/2} \times \exp\left(-\frac{1}{2} \lambda_n^{-1} (\eta_n - \eta_{n,c})^2 \right) \exp(-\mu_n \nu_n^2) \quad (25)$$

which is normalized except for a factor of $(2\pi\hbar)^{-3N}$, canceling the factor in front of eq 1. To evaluate $W(q,p)$, eqs 21−23 are utilized. The remaining part of eq 18 is multiplied together with eq 17 to yield the CF to be averaged. In the actual simulation, we implemented the *complex conjugate* of eq 10, which is just eqs 17−18 with i replaced by $-i$. Before closing this section, we mention, as shown in the Appendix, that the first moment of $S(\vec{Q},\omega)$ (eq 13) is reproduced exactly by the FK-LPI theory.

3. FK-LPI Molecular Dynamics Simulation

To calculate the Van Hove CF at $T = 27$ K (the actual temperature used in the simulation was 26.65 K, which we will refer to as 27 K) and a density of 0.25 g/cm^3, we consider 64 He(4) atoms each with mass 7301 au in a cubic simulation box of length $L = 22.562$ bohr. This box is then replicated to produce an infinite system using periodic boundary conditions.[1] The experimental Q vector is: $Q = 1.64$ Å$^{-1} = 0.87$ bohr^{-1}.[34] For a macroscopic liquid, one only gets a diffracted beam provided the Laue equation is fulfilled[19]

$$L \times Q = n2\pi \quad (26)$$

for some integer n. For our boxlength, the allowed Q values are 0.28, 0.56, 0.84 bohr^{-1}, etc. We have, however, utilized $Q = 0.87$ bohr^{-1} in our calculations. In a more ambitious study, one should vary the number of particles and boxlength to exactly match the Laue equation and density simultaneously. To model the He(4)−He(4) interaction, the highly accurate HFD-B2 pair potential of Aziz and co-workers[3] was adopted together with the standard minimum image convention and a potential cutoff at half boxlength.[1] To allow an analytical evaluation of certain results (see eq 50 in ref 26), the Aziz pair potential was represented accurately as a sum of three Gaussian functions

$$V_{He-He}^{Aziz}(r) = \sum_{i=1}^{3} \gamma_i \exp\left(-\frac{1}{2} r^2/\alpha_i \right) \quad (27)$$

The coefficient values are collected in Table 1. A Monte Carlo (MC) walk of 300 000 steps in the centroid position, r_c, was generated using the centroid density $\rho_{FK}(r_c)$ employing an average acceptance probability of 40%. For a description of how to generate the FK centroid density and its associated effective frequencies, we refer to the literature.[7,26] At each tenth MC step, 10 samples of phase-space points (q,p) were generated from the sampling function in eq 25. These were then propagated classically for 11.7 ps using velocity Verlet[1] with a time step of 11.4 fs. From these trajectories, the Van Hove correlation function was constructed, as sketched in the previous section, by utilizing the 64 He(4) atoms in the central simulation box. The entire Van Hove calculation (Monte Carlo plus classical dynamics) took approximately three weeks on a single PC with a 2.0-GHz processor.

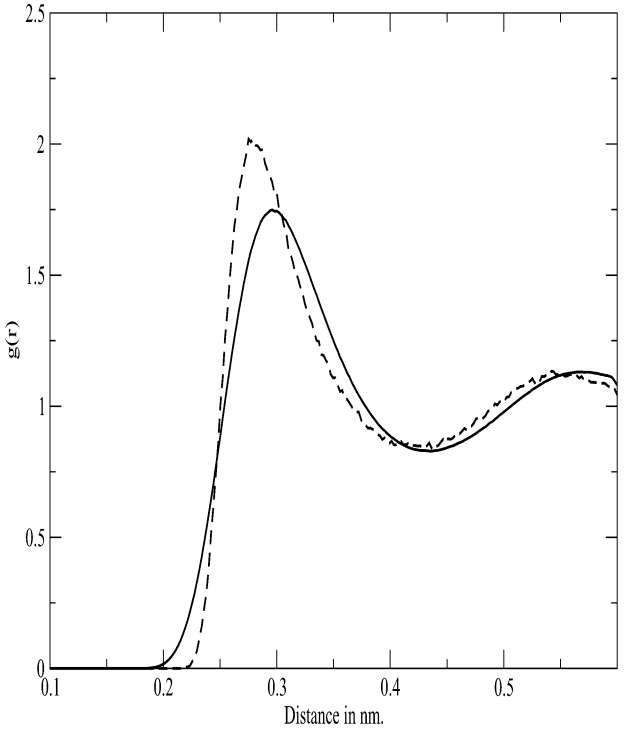

Figure 1. Radial distribution functions for He(4) at $T = 27$ K and density 0.25 g/cm^3. Solid line, Wigner; dashed line, classical.

TABLE 1: Gaussian Parameters for the He(4)−He(4) Aziz Interaction Potential

i	α_i/bohr^2	γ_i/Hartree
1	0.891553	0.615
2	9.1628	−0.000237363
3	1.62309	0.131044

4. Results

4.1. Structural Properties. The semianalytical Wigner transform contains all information on the structural properties of the He(4) liquid. A sensible way of checking the quality of the approximate transform is to compare with accurately known structural properties of He(4). One is the kinetic energy of liquid He(4). By utilizing the path integral Monte Carlo (PIMC) based kinetic energy contour plot of Ceperley and co-workers,[8] we obtain an accurate theoretical value of the kinetic energy per particle at our thermodynamic point. From the data of ref 8, the value is seen to be 61−62 K. From our approximate Boltzmann Wigner transform, we get 62.7 ± 0.3 K, which is in very good accord with Ceperley et al., especially if one compares with the classical value of $1.5 \times T = 40.5$ K. We have also computed the radial distribution function, $g(r)$, for He(4) both by FK-LPI and classically, see Figure 1. We see a substantial change in the structure of the liquid; indeed the quantum particles are able to approach each other more closely (as close as ∼0.20 nm), which should be compared with the classical minimum distance of ∼0.23 nm. We have not been able to find radial distribution functions from PIMC/experiment at our thermodynamic point, but the lower limit of ∼0.20 nm is in quantitative agreement with PIMC-based $g(r)$s at other low-temperature thermodynamic points, see ref 8.

In Figure 2, the effective-frequency distribution is shown. By convention, imaginary frequencies, associated with unstable normal modes, are shown on the negative frequency axis. As is clearly seen, they represent a significant part of the spectrum.

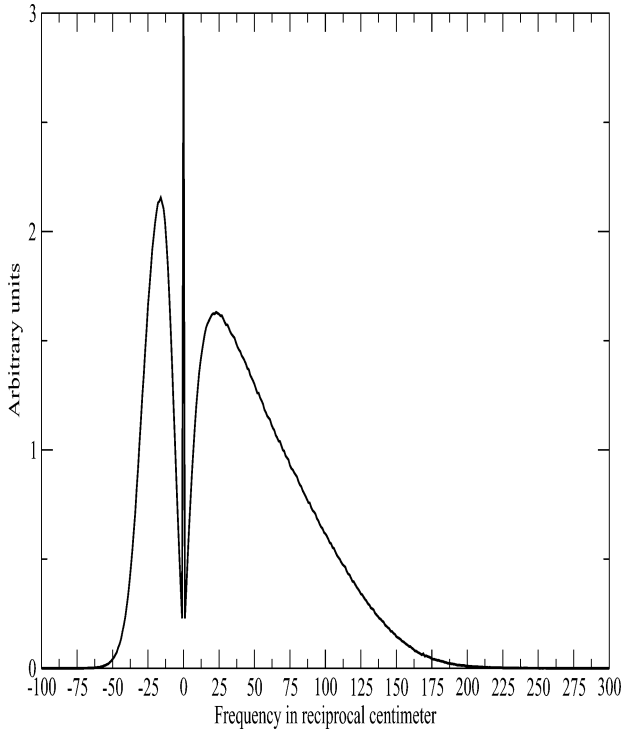

Figure 2. Effective-frequency distribution for He(4) at $T = 27$ K and density 0.25 g/cm^3.

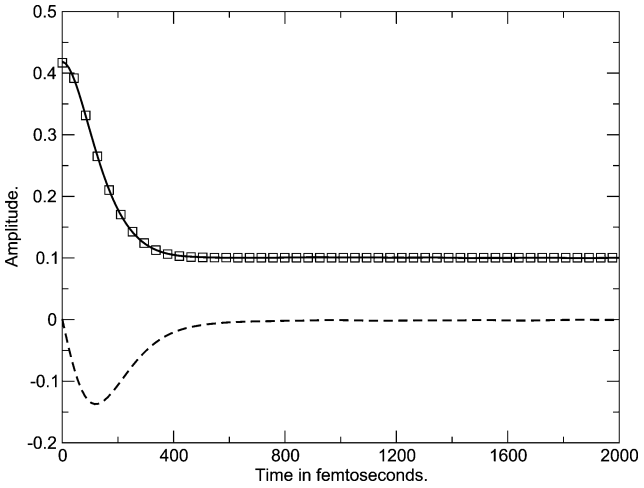

Figure 3. Complex conjugated Van Hove CF at $T = 27$ K and density 0.25 g/cm^3. Solid line, FK-LPI CF (real part); dashed line, FK-LPI CF (imaginary part); □, Gaussian fit.

However, we note here that these imaginary frequencies do not present a problem in the present context. As discussed in ref 26, the equations are well behaved as long as $\hbar|\Omega_n(r_c)| < \pi k_B T$. At 27 K, this cutoff occurs at 59 cm^{-1}. Hence, it is evident from the data in Figure 2 that there is only a very small component of the imaginary wing outside this range. For large magnitude imaginary frequencies, we use the convention[26] that the value of ν_n (cf. eq 18) is chosen the same as that reached as the cutoff is approached, namely, $\nu_n = 0$.

4.2. Van Hove Correlation Function. In Figure 3, we show the calculated real and imaginary parts of the complex conjugated Van Hove CF. Also is shown a fit to the real part using a sum of Gaussian functions. We note the relatively large imaginary part of the CF, which vanishes classically, thereby showing the true quantum character of the Helium liquid. Also it is seen that the real part of the CF reaches a constant nonzero plateau for long times; this is a direct consequence of the fact

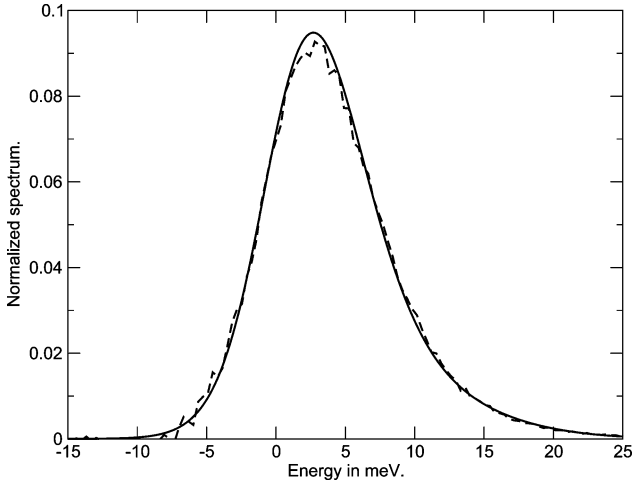

Figure 4. Normalized Van Hove spectrum for He(4) at $T = 27$ K and density 0.25 g/cm^3. Solid line, FK-LPI (eq 30); dashed line, FK-LPI (eq 11).

that the Laue equation is not exactly fulfilled. The plateau value (t large)

$$S(\vec{Q},t) = \frac{1}{N}\langle\sum_{j=1}^{N}\exp(-iQr_j)\rangle\langle\sum_{j=1}^{N}\exp(iQr_j)\rangle \equiv \frac{\langle\Sigma\rangle^2}{N} \tag{28}$$

can be removed by considering the alternative CF

$$\tilde{S}(\vec{Q},t) = \frac{1}{N}\sum_{j,k=1}^{N}\left\langle\left[\exp(-i\vec{Q}\vec{r}_j(0)) - \frac{1}{N}\langle\Sigma\rangle\right]\times \left[\exp(i\vec{Q}\vec{r}_k(t)) - \frac{1}{N}\langle\Sigma\rangle\right]\right\rangle \tag{29}$$

However, as is easily shown, the difference between the FK-LPI implementations of eqs 10 and 29 is just an irrelevant additive constant. This follows from the stationarity of $\langle\sum_{j=1}^{N}\exp(iQr_j(t))\rangle$ in the FK-LPI simulation due to the uniform single-particle position probability density. The plateau value adds to the zero-frequency Fourier mode of the Van Hove spectrum, and we have chosen to remove it when computing the spectrum via eq 11 or eq 30. We have calculated the spectrum in two different ways. The first is the "direct" way, based on eq 11, where one utilizes the full CF (real plus imaginary part) depicted in Figure 3. The other way is less direct but numerically more appealing. One makes use of the analytical Gaussian fit to the real part of the CF and computes the Van Hove spectrum analytically by exploiting the formal identity (derived from detailed balance) employing the real part of the CF only

$$S(\vec{Q},\omega) = \frac{1}{2\pi}\frac{2}{1+\exp(-\beta\hbar\omega)}\int_{-\infty}^{+\infty} dt\,\exp(-i\omega t)Real\{S(\vec{Q},t)\} \tag{30}$$

The spectrum computed via eq 30 with a Gaussian fit will predictably produce a smooth result. In Figure 4, we show the calculated spectrum using eqs 11 and 30. Very good agreement is clearly observed, indicating that the FK-LPI method, for this system, works consistently and that detailed balance is fulfilled when utilizing the "direct" method based solely on eq 11.

The calculated spectrum from eq 30 should be convoluted with the experimental instrument response, thereby yielding a spectrum which could be compared with experiment.[34] Such a convolution however turns out to only have a negligible effect

TABLE 2: Moments of $S(\vec{Q},\omega)$ for $||\vec{Q}|| = 1.64$ Å^{-1}, $T = 27$ K and Density 0.25 g/cm^3 [a]

	exp[34]	FK-LPI	exact/accurate theory[34]	classical
$\hbar\langle\omega\rangle$/cm^{-1} (eq 13)		10.4 ± 0.4	11.37	0.
$\tilde{R}^2$ (eq 15)	1.8	1.71 ± 0.05		1.
R^3/meV^2 (eq 14)	165 ($Q = 1.67$ Å^{-1})	106 ± 7	123 ($Q = 1.63$ Å^{-1})	

[a] Column numbers 2−5 refer to moments derived from: (2) experiment, (3) FK-LPI theory, (4) accurate theory, and (5) classical dynamics, respectively.

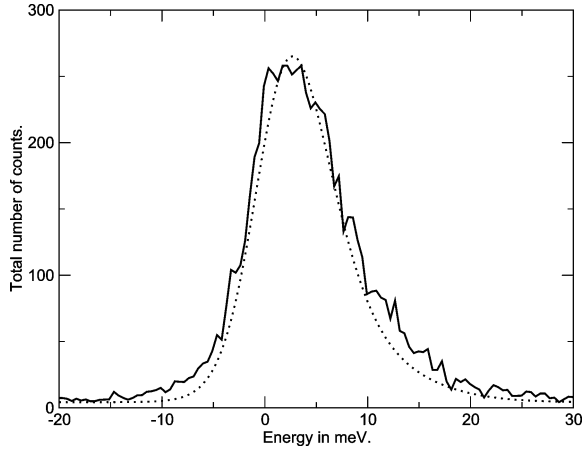

Figure 5. Experimental and theoretical IXS spectra for He(4) at $T = 27$ K and density 0.25 g/cm^3. Dotted Line, FK-LPI; solid line, experimental.

(A. Cunsolo, private communication) and is not included in Figure 5, which shows the experimental and theoretical spectra. Good agreement is clearly observed, especially for the widths of the two spectra.

On the basis of a viscoelastic model, Verbeni and co-workers[34] calculated the second (reduced) and third moments of $S(\vec{Q},\omega)$. In Table 2, we compare these experimental moments with those derived from eq 30. Some comments are appropriate: First, the exact first moment is calculated from eq 13. Moreover, the value of the experimental reduced second moment is obtained by interpolating the data of Figure 5 in ref 34. The value given for the accurate third moment was calculated by Verbeni and co-workers[34] by utilizing an expression for R^3 that is exact for a purely pairwise additive potential.[27] The expression requires the He(4)−He(4) radial distribution function, pair potential, and liquid kinetic energy. To evaluate this expression, Verbeni and co-workers employed experimental radial distribution functions, the Aziz potential[2] and the accurate kinetic energies of Ceperley and co-workers.[8] From Table 2, one observes a very good agreement between the FK-LPI first and second moments and those derived from theory or experiment. In fact our reduced second moment is in better agreement with experiment than a reduced second moment derived from a truncated $\hbar$ expression (see Figure 6 of ref 34), yielding a reduced second moment of $\simeq 2.25$. When comparing the third moments, we see a somewhat larger disagreement between experiment and FK-LPI. However, as is obvious from Figure 7 of ref 34, there is a considerable amount of uncertainty in the determination of cubic moments for Q values above $\sim$15 nm^{-1}. The good agreement between FK-LPI and the accurate theoretical result evident in Table 2 suggests that the current value is indeed reasonable.

5. Discussion and Conclusion

We have applied the semiclassical linearized path integral methodology to the problem of determining the Van Hove correlation function for liquid He(4) at 27 K and a density of 0.25 g/cm^3. Also the He(4) kinetic energy was calculated. As this system is anharmonic and the CF considered is highly nonlinear, this is a challenging test. All of these quantities were found to be in very good agreement with experiment and accurate theory. In particular, the close agreement between the accurate PIMC-based kinetic energy and the energy predicted by FK-LPI is a direct verification of the accuracy of the approximate Wigner transform of ref 26, for this system.

It is interesting to speculate on why the LPI approximation, or equivalently, the CW model, works so well for He(4) at this thermodynamic point. Why is classical dynamics good enough for propagating the Wigner-transformed free-particle Heisenberg operator? One could speculate that the high density (equivalent to a pressure of 3−4 kbar)[34] makes the liquid solidlike and henceforth harmonic. Since the CW model is exact for harmonic potentials, this would explain matters. This argument can however be ruled out by observing the large fraction of unstable modes in Figure 2, and noting that the presence of these discriminates a liquid from a solid. Hence, He(4) at our thermodynamic point is not at all solidlike. As noted in ref 26, if decoherence is strong enough, classical equations of motion suffice for the evolution of the Wigner transformed operators. We are confident that decoherence *is* of key importance for the accuracy of the FK-LPI approach to the dynamics in the He(4) liquid. However, lacking a quantitative measure of decoherence, we are limited to a qualitative discussion at this point. In this respect, it is interesting to notice that, for harmonic models, the decoherence functional[5,11] can be explicitly constructed, thereby opening up the possibility of a quantitative measure of decoherence. One could produce an approximate decoherence functional for general liquids based on the effective frequencies and their associated normal modes.

Another issue is how harmonic/anharmonic is the dynamics that are being probed? For example, the value of a diffusion coefficient, which monitors motion over barriers, depends strongly on anharmonic effects and is in fact zero for a strictly harmonic model (e.g., a solid). On the other hand, the Van Hove CF measures density fluctuations which are present also in a harmonic solid and one concludes that this CF, for such a system, is completely dominated by harmonic motion. To what extent the liquid He(4) Van Hove CF is harmonic in character requires a separate investigation but on qualitative grounds, we should expect the CW/LPI approach to be more suitable for determining Van Hove CFs than, e.g., diffusion coefficients.

To summarize, the FK-LPI theory has been shown to work extremely well for determining the Van Hove spectrum of liquid He(4). Further studies are clearly needed to gain a more complete knowledge of its range of validity.

Acknowledgment. This work is dedicated to the late Professor Gert Due Billing whose original contributions to the field of molecular dynamics have inspired us all. J.A.P. and G.N. gratefully acknowledges support from both the Danish Natural Science Research Council and the Swedish Research council. P.J.R. gratefully acknowledges support by the National Science Foundation (CHE-0134775) and the Robert A. Welch Foundation. J.A.P. is greately indebted to Professors G. Ciccotti and D. Coker for informative discussions concerning various aspects of the molecular dynamics simulation. J.A.P also thanks G. Ruocco and A. Cunsolo for performing the convolution of

a preliminary theoretical IXS spectrum and for making their experimental data accessible to the authors.

Appendix A

Here we derive eq 18 and show that the first moment of $S(\vec{Q},\omega)$ is exactly given by FK-LPI theory. First, we derive the multidimensional version of the Feynman−Kleinert quasidensity operator (QDO) in eq 5

$$\hat{\delta}_{\mathrm{FK}}(r_c,p_c) = \int\int \mathrm{d}x\,\mathrm{d}x' \left(\frac{M\Omega(r_c)}{\pi\hbar\alpha}\right)^{1/2} |x'\rangle\langle x| \exp\left(i\frac{p_c}{\hbar}(x'-x) - \frac{M\Omega(r_c)}{\hbar\alpha}\left(\frac{x+x'}{2}-r_c\right)^2 - \frac{M\Omega(r_c)\alpha}{4\hbar}(x'-x)^2\right) \quad (31)$$

To proceed, we first transform eq 31 to a mass-weighted normal-mode representation, via eqs 21−24

$$\hat{\delta}_{\mathrm{FK}}(r_c,p_c) = \int\int \mathrm{d}\eta\,\mathrm{d}\eta' \left(\frac{\Omega(r_c)}{\pi\hbar\alpha}\right)^{1/2} |\eta'\rangle\langle\eta| \exp\left(i\frac{\nu_c}{\hbar}(\eta'-\eta) - \frac{\Omega(r_c)}{\hbar\alpha}\left(\frac{\eta+\eta'}{2}-\eta_c\right)^2 - \frac{\Omega(r_c)\alpha}{4\hbar}(\eta'-\eta)^2\right) \quad (32)$$

Equation 32 is the QDO of a harmonic oscillator of frequency $\Omega(r_c)$.[17] It is easily generalized to the multidimensional case, where it simply becomes the direct product of $3N$ one-dimensional normal-mode QDOs each one in a form identical to eq 32. As in section 2.4, η, λ, q, p, r_c, p_c, η_c, and ν_c will in the following denote $3N$ dimensional vectors. The multidimensional QDO expressed in mass-weighted normal modes is accordingly

$$\hat{\delta}_{\mathrm{FK}}(r_c,p_c) = \prod_{k=1}^{3N} \int\int \mathrm{d}\eta_k\,\mathrm{d}\eta_k' \left(\frac{\Omega_k(r_c)}{\pi\hbar\alpha_k}\right)^{1/2} |\eta_k'\rangle\langle\eta_k| \exp\left(i\frac{\nu_{c,k}}{\hbar}(\eta_k'-\eta_k) - \frac{\Omega_k(r_c)}{\hbar\alpha_k}\left(\frac{\eta_k+\eta_k'}{2}-\eta_{c,k}\right)^2 - \frac{\Omega_k(r_c)\alpha_k}{4\hbar}(\eta_k'-\eta_k)^2\right) \quad (33)$$

Next, we write the general many-dimensional Wigner transform, defined in eq 2, also in mass-weighted normal modes. Using eqs 21−24, we obtain

$$(\hat{C})_{\mathrm{W}}[q,p] \equiv \int_{-\infty}^{+\infty} \mathrm{d}\lambda\, \exp(i\tilde{p}\lambda/\hbar)\left\langle \tilde{q}+\frac{1}{2}\lambda\middle|\hat{C}\middle|\tilde{q}-\frac{1}{2}\lambda\right\rangle \quad (34)$$

where λ is a mass-weighted normal-mode coordinate vector and $(\tilde{q},\tilde{p})$ is the normal mode analogues of the sampled position and momentum vectors (q,p)

$$\tilde{q} = \mathbf{U}^{\dagger}(r_c)\mathbf{M}^{1/2}q \quad (35)$$

and

$$\tilde{p} = \mathbf{U}^{\dagger}(r_c)\mathbf{M}^{-1/2}p \quad (36)$$

To derive eq 18, we rewrite the free particle operator ($\vec{Q}$ is chosen along the x axis)

$$\sum_{j=1}^{N} \exp(-i\vec{Q}\vec{r}_j) = \sum_{j=1}^{N} \exp(-iQr_j) = \sum_{j=1}^{N} \exp(-iQ[\mathbf{M}^{-1/2}\mathbf{U}(r_c)\eta]_{3(j-1)+1}) \quad (37)$$

where Q is the norm of $\vec{Q}$, r_j is the x-coordinate operator of atom j, and η_i is the ith mass-weighted normal-mode coordinate, see eq 21. We may now write

$$(\hat{\delta}_{\mathrm{FK}}(r_c,p_c)\sum_{j=1}^{N}\exp(-iQr_j))_{\mathrm{W}}[q,p] = \int_{-\infty}^{+\infty}\mathrm{d}\lambda\,\exp(-i\tilde{p}\lambda/\hbar)\sum_{j=1}^{N}\left\langle\tilde{q}+\frac{1}{2}\lambda\middle|\,\hat{\delta}_{\mathrm{FK}}(r_c,p_c)\times \exp(-iQ[\mathbf{M}^{-1/2}\mathbf{U}(r_c)\eta]_{3(j-1)+1})\middle|\tilde{q}-\frac{1}{2}\lambda\right\rangle \quad (38)$$

$$= \int_{-\infty}^{+\infty}\mathrm{d}\lambda\,\exp(-i\tilde{p}\lambda/\hbar)\left\langle\tilde{q}+\frac{1}{2}\lambda\middle|\,\hat{\delta}_{\mathrm{FK}}(r_c,p_c)\middle|\,\tilde{q}-\frac{1}{2}\lambda\right\rangle\sum_{j=1}^{N}\exp\left(\frac{i}{2}Q[\mathbf{M}^{-1/2}\mathbf{U}(r_c)\lambda]_{3(j-1)+1}\right)\exp(-iQq_j) \quad (39)$$

By inserting the expression for $\hat{\delta}_{\mathrm{FK}}(r_c,p_c)$ in eq 33, we obtain

$$(\hat{\delta}_{\mathrm{FK}}(r_c,p_c)\sum_{j=1}^{N}\exp(-iQr_j))_{\mathrm{W}}[q,p] = \int_{-\infty}^{+\infty}\mathrm{d}\lambda\,\exp(-i\tilde{p}\lambda/\hbar)\sum_{j=1}^{N}\exp\left(\frac{i}{2}Q[\mathbf{M}^{-1/2}\mathbf{U}(r_c)\lambda]_{3(j-1)+1}\right)\times \exp(-iQq_j)\prod_{k=1}^{3N}\left(\frac{\Omega_k(r_c)}{\pi\hbar\alpha_k}\right)^{1/2}\times \exp\left(i\frac{\nu_{c,k}}{\hbar}\lambda_k - \frac{\Omega_k(r_c)}{\hbar\alpha_k}(\tilde{q}_k-\eta_{c,k})^2 - \frac{\Omega_k(r_c)\alpha_k}{4\hbar}{\lambda_k}^2\right) \quad (40)$$

By performing the integral over the λ vector, we further get

$$(\hat{\delta}_{\mathrm{FK}}(r_c,p_c)\sum_{j=1}^{N}\exp(-iQr_j))_{\mathrm{W}}[q,p] = \sum_{j=1}^{N}\exp(-iQq_j)\prod_{k=1}^{3N}\frac{2}{\alpha_k}\exp\left(-\frac{\Omega_j(r_c)}{\hbar\alpha_j}(\tilde{q}_j-\eta_{c,k})^2\right)\times \exp\left(-\frac{1}{\hbar\Omega_k(r_c)\alpha_k}\left(\nu_{c,k}-\tilde{p}_k+\frac{\hbar}{2}Qm_j^{-1/2}\mathbf{U}(r_c)_{3(j-1)+1,k}\right)^2\right) \quad (41)$$

Next we consider the expression

$$\int\int \mathrm{d}r_c\,\mathrm{d}p_c\,\rho_{\mathrm{FK}}(r_c,p_c)(\hat{\delta}_{\mathrm{FK}}(r_c,p_c)\sum_{j=1}^{N}\exp(-iQr_j))_{\mathrm{W}}[q,p] \quad (42)$$

From the formula for $\rho_{\mathrm{FK}}(r_c,p_c)$ in eq 4, we see that eq 42 is quadratic in p_c, or equivalently, ν_c. Integrating this vector out in eq 42 yields

$$\int\int \mathrm{d}r_c\, \mathrm{d}p_c\, \rho_{FK}(r_c,p_c)(\hat{\delta}_{FK}(r_c,p_c)\sum_{j=1}^{N}\exp(-iQr_j))_W[q,p] = \int \mathrm{d}r_c \frac{\det(\mathbf{M}^{1/2})}{(2\pi\hbar)^{3N}}\exp(-\beta W_1(r_c))\sum_{j=1}^{N}\exp(-iQq_j)\times \prod_{k=1}^{3N}\frac{2}{\alpha_k}\left(\frac{\alpha_k\pi}{\frac{\beta}{2}\coth\left(\frac{\hbar\Omega_k(r_c)\beta}{2}\right)}\right)^{1/2}\exp\left(-\frac{\Omega_k(r_c)}{\hbar\alpha_k}(\tilde{q}_k-\eta_{c,k})^2\right)\times \exp\left(-\frac{\tanh(\hbar\Omega_k(r_c)\beta/2)}{\Omega_k(r_c)\hbar}\left(\tilde{p}_k-\frac{\hbar}{2}Qm_j^{-1/2}\mathbf{U}(r_c)_{3(j-1)+1,k}\right)^2\right) \quad (43)$$

or

$$\int\int \mathrm{d}r_c\, \mathrm{d}p_c\, \rho_{FK}(r_c,p_c)(\hat{\delta}_{FK}(r_c,p_c)\sum_{j=1}^{N}\exp(-iQr_j))_W[q,p] = \int \mathrm{d}r_c \frac{\det(\mathbf{M}^{1/2})}{(2\pi\hbar)^{3N}}\rho_{FK}(r_c)\sum_{j=1}^{N}\exp(-iQq_j)\times \prod_{k=1}^{3N}\frac{2}{\alpha_k}\left(\frac{\alpha_k\pi}{\frac{\beta}{2}\coth\left(\frac{\hbar\Omega_k(r_c)\beta}{2}\right)}\right)^{1/2}\times \exp\left(-\frac{\Omega_k(r_c)}{\hbar\alpha_k}(\tilde{q}_k-\eta_{c,k})^2-\frac{\tanh(\hbar\Omega_k(r_c)\beta/2)}{\Omega_k(r_c)\hbar}\tilde{p}_k^{\,2}\right)\times \exp\left(\frac{\tanh(\hbar\Omega_k(r_c)\beta/2)}{\Omega_k(r_c)}\tilde{p}_k Qm_j^{-1/2}\mathbf{U}(r_c)_{3(j-1)+1,k}\right)\times \exp\left(-\frac{\hbar\tanh(\hbar\Omega_k(r_c)\beta/2)}{4\Omega_k(r_c)}(Qm_j^{-1/2}\mathbf{U}(r_c)_{3(j-1)+1,k})^2\right) \quad (44)$$

This completes the proof of eq 18.

Next we proceed to derive the first moment rule in eq 13. Again, the $\vec{Q}$ vector lies along the x axis. We start by observing that from the inverse of eq 11

$$S(\vec{Q},t) = \int_{-\infty}^{+\infty}\mathrm{d}\omega\, \exp(i\omega t)S(\vec{Q},\omega) \quad (45)$$

we obtain

$$\frac{\mathrm{d}}{\mathrm{d}t}S(\vec{Q},t)|_{t=0} = i\int_{-\infty}^{+\infty}\mathrm{d}\omega\, \omega S(\vec{Q},\omega) \quad (46)$$

or from eq 12

$$\langle\omega\rangle = -i\frac{\mathrm{d}}{\mathrm{d}t}S(\vec{Q},t)|_{t=0} \quad (47)$$

From eq 1, the FK-LPI approximation to eq 47 is

$$\langle\omega\rangle = \frac{1}{Z_{FK}N}\frac{1}{(2\pi\hbar)^{3N}}\int \mathrm{d}r_c\, \mathrm{d}p_c\, \rho_{FK}(r_c,p_c)\times \int \mathrm{d}q\, \mathrm{d}p\, (\hat{\delta}_{FK}(r_c,p_c)\sum_{i,j=1}^{N}\exp(-iQr_j))_W[q,p]\frac{Qp_i}{m_i}\exp(iQq_i) \quad (48)$$

where p_i is the x component of the sampled momentum pertaining to particle i. Utilizing eq 43, we obtain

$$\langle\omega\rangle = \frac{1}{Z_{FK}N}\frac{1}{(2\pi\hbar)^{3N}}\int \mathrm{d}r_c\int \mathrm{d}q\, \mathrm{d}p\frac{\det(\mathbf{M}^{1/2})}{(2\pi\hbar)^{3N}}\times \exp(-\beta W_1(r_c))\sum_{i,j=1}^{N}\left\{\prod_{k=1}^{3N}\frac{2}{\alpha_k}\left(\frac{\alpha_k\pi}{\frac{\beta}{2}\coth\left(\frac{\hbar\Omega_k(r_c)\beta}{2}\right)}\right)^{1/2}\times \exp\left(-\frac{\Omega_k(r_c)}{\hbar\alpha_k}(\tilde{q}_k-\eta_{c,k})^2\right)\exp\left(-\frac{\tanh(\hbar\Omega_k(r_c)\beta/2)}{\Omega_k(r_c)\hbar}\times \left(\tilde{p}_k-\frac{\hbar}{2}Qm_j^{-1/2}\mathbf{U}(r_c)_{3(j-1)+1,k}\right)^2\right)\right\}Q\frac{p_i}{m_i}\exp(-iQq_j)\exp(iQq_i) \quad (49)$$

Next, transform the p variable into the mass-weighted momentum vector, $\tilde{p}$, using eq 36. After integrating this vector out, eq 49 becomes

$$\langle\omega\rangle = \frac{1}{Z_{FK}N}\frac{1}{(2\pi\hbar)^{3N}}\int \mathrm{d}r_c\int \mathrm{d}q\frac{\det(\mathbf{M})}{(2\pi\hbar)^{3N}}\times \exp(-\beta W_1(r_c))\sum_{i,j=1}^{N}\frac{\hbar Q^2}{2m_i}\exp(-iQq_j)\times \exp(iQq_i)\, m_j^{-1/2}m_i^{1/2}\sum_{l=1}^{3N}\mathbf{U}(r_c)_{3(i-1)+1,l}\mathbf{U}(r_c)_{3(j-1)+1,l}\times \prod_{k=1}^{3N}\frac{2}{\alpha_k}\left(\frac{\alpha_k\pi^2\Omega_k(r_c)\hbar}{\frac{\beta}{2}}\right)^{1/2}\exp\left(-\frac{\Omega_k(r_c)}{\hbar\alpha_k}(\tilde{q}_k-\eta_{c,k})^2\right) \quad (50)$$

Since $\mathbf{U}^{-1}(r_c) = \mathbf{U}^{\dagger}(r_c)$, we have

$$\sum_{l=1}^{3N}\mathbf{U}(r_c)_{3(i-1)+1,l}\mathbf{U}(r_c)_{3(j-1)+1,l} = \sum_{l=1}^{3N}\mathbf{U}(r_c)_{3(i-1)+1,l}\mathbf{U}^{\dagger}(r_c)_{l,3(j-1)+1} = \delta_{ij} \quad (51)$$

and accordingly, we may impose the restriction $i = j$. The remaining integrations over q and r_c cancel the partition function Z_{FK}, leaving us with

$$\langle\omega\rangle = \frac{\hbar Q^2}{2M_{He(4)}} \quad (52)$$

as was to be proved.

References and Notes

(1) Allen, M. P.; Tildesley, D. J. *Computer Simulations of Liquids*; Oxford University Press: Oxford, 1987.
(2) Aziz, R. A.; Nain, V. P. S.; Carly, J. S.; Taylor, W. L.; McConville, G. T. *J. Chem. Phys.* **1979**, *70*, 4330.
(3) Aziz, R. A.; Slaman, M. J.; Koide, A.; Allnatt, A. R.; Meath, W. J. *Mol. Phys.* **1992**, *77*, 321−337.
(4) Boninsegni, M.; Ceperley, D. M. *J. Low Temp. Phys.* **1996**, *104*, 339.
(5) Caldeira, A. O.; Leggett, A. J. *Physica* **1983**, *121A*, 587−616.
(6) Calhoun, A.; Pavese, M.; Voth, G. A. *Chem. Phys. Lett.* **1999**, *262*, 415.

(7) Cao, J.; Voth, G. A. *J. Chem. Phys.* **1994**, *101*, 6168−6183.
(8) Ceperley, D. M.; Simmons, R. O.; Blasdell, R. C. *Phys. Rev. Lett.* **1997**, *77*, 115−118.
(9) Ciccotti, G.; Pierleoni, C.; Capuani, F.; Filinov, V. S. *Comput. Phys. Commun.* **1999**, *121*−*122*, 452−459.
(10) Feynman, R. P.; Kleinert, H. *Phys. Rev. A* **1986**, *34*, 5080−5084.
(11) Gell-Mann, M.; Hartle, J. B. *Phys. Rev. D* **1993**, *47*, 3345.
(12) Giachetti, R.; Tognetti, V. *Phys. Rev. Lett.* **1985**, *55*, 912−915.
(13) Giachetti, R.; Tognetti, V. *Phys. Rev. B* **1986**, *33*, 7647−7658.
(14) Giulini, D.; Joos, E.; Kiefer, C.; Kupsch, J.; Stamatescu, I.-O.; Zeh, H. D. *Decoherence and the Appearance of a Classical World in Quantum Theory*; Springer-Verlag: Berlin, 1996.
(15) Husimi, K. *Proc. Phys. Math. Soc. Jpn.* **1940**, *22*, 264−314.
(16) Jang, S.; Pak, Y.; Voth, G. A. *J. Phys. Chem. A* **1999**, *103*, 10289−10293.
(17) Jang, S.; Voth, G. A. *J. Chem. Phys.* **1999**, *111*, 2357.
(18) Kinugawa, K. *Chem. Phys. Lett.* **1998**, *292*, 454−460.
(19) Kittel, C. *Introduction to solid-state physics*; John Wiley and Sons: New York, 1966.
(20) Kleinert, H. *Path Integrals in Quantum Mechanics, Statistics and Polymer Physics*; World Scientific: Singapore, 1995.
(21) Lobaugh, J.; Voth, G. A. *J. Chem. Phys.* **1996**, *106*, 2400.
(22) March, N. H.; Young, W. H.; Sampanthar, S. *The Many-Body Problem in Quantum Mechanics*; Dover Publications: New York, 1995.
(23) Miller, W. H. *J. Phys. Chem. A* **2001**, *105*, 2942−2955.
(24) Miura, S.; Okazaki, S.; Kinugawa, K. *J. Chem. Phys.* **1999**, *110*, 4523−4532.
(25) Nakayama, A.; Makri, N. *J. Chem. Phys.* **2003**, *119*, 8592−8605.
(26) Poulsen, J. Aa.; Nyman, Rossky, P. J. *J. Chem. Phys.* **2003**, *119*, 12179−12193.
(27) Puff, R. D. *Phys. Rev.* **1965**, *137*, A406.
(28) Rabani, E.; Reichman, D. R.; Krilov, G.; Berne, B. J. *Proc. Natl. Acad. Sci.* **2002**, *99*, 1129−1133.
(29) Reichman, D. R.; Rabani, E. *J. Chem. Phys.* **2002**, *116*, 6279−6285.
(30) Shi, Q.; Geva, E. *J. Phys. Chem. B* **2003**, *107*, 9059−9069.
(31) Shi, Q.; Geva, E. *J. Phys. Chem. B* **2003**, *107*, 9070−9078.
(32) Shi, Q.; Geva, E. *J. Chem. Phys.* **2003**, *118*, 8173.
(33) Sun, X.; Wang, H.; Miller, W. H. *J. Chem. Phys.* **1998**, *109*, 7064−7073.
(34) Verbeni, R.; Cunsolo, A.; Pratesi, G.; Monaco, G.; Rosica, F.; Masciovecchio, C.; Nardone, M.; Ruocco, G.; Sette, F.; Albergamo, F. *Phys. Rev. E* **2001**, *64*, 021203.
(35) Wang, H.; Sun, X.; Miller, W. H. *J. Chem. Phys.* **1998**, *108*, 9726−9736.
(36) Wright, N. J.; Makri, N. *J. Chem. Phys.* **2003**, *119*, 1634−1641.
(37) Yonetani, Y.; Kinugawa, K. *J. Chem. Phys.* **2003**, *119*, 9651−9660.